

PAPER

Nano-diamond based spheres for radio frequency electromechanical resonators

To cite this article: V Lebedev *et al* 2014 *J. Micromech. Microeng.* **24** 045015

View the [article online](#) for updates and enhancements.

You may also like

- [Diamond—the ultimate material for exploring physics of spin-defects for quantum technologies and diamondtronics](#)
Dhruba Das, Rahul Raj, Jayanta Jana et al.
- [Phosphorylated nano-diamond/ Polyimide Nanocomposites](#)
Asli Beyler-Çiil, Emrah Çakmakçı and Memet Vezir Kahraman
- [Piezoelectric actuated micro-resonators based on the growth of diamond on aluminum nitride thin films](#)
J Hees, N Heidrich, W Pletschen et al.



ECS
The
Electrochemical
Society
Advancing solid state &
electrochemical science & technology

DISCOVER
how sustainability
intersects with
electrochemistry & solid
state science research

Nano-diamond based spheres for radio frequency electromechanical resonators

V Lebedev¹, D Iankov^{1,2}, N Heidrich¹, V Zuerbig^{1,2}, C Wild³, V Cimalla¹
and O Ambacher^{1,2}

¹ Fraunhofer Institute for Applied Solid State Physics, Tullastraße 72, D-79108 Freiburg, Germany

² IMTEK, University of Freiburg, Georges-Köhler-Allee 106, D-79110 Freiburg, Germany

³ Diamond Materials GmbH, Hans-Bunte-Str. 19, D-79108 Freiburg, Germany

E-mail: vadim.lebedev@iaf.fraunhofer.de

Received 25 November 2013, revised 18 January 2014

Accepted for publication 5 February 2014

Published 25 March 2014

Abstract

In this work, we report on the electro-mechanical studies of high- Q spherical oscillators designed to operate in radio-frequency circuits. Resonating composite spheres, consisting of a silicon core and a thick nanodiamond shell, were studied by laser vibrometry in order to obtain mechanical quality factors and identify the resonant frequencies and eigenmodes of the system. Finite element method simulations were used to analyze and confirm the experimental data. Additionally, reflection/transmission measurements were carried out on capacitively coupled spheres in order to evaluate the electrical parameters of the system. The main aim of these investigations was to evaluate the potential of diamond-based spherical resonators to be used in modern communication devices.

Keywords: nanodiamond, MEMS, resonator, transducer

(Some figures may appear in colour only in the online journal)

1. Introduction

The rapid evolution of wireless communications is generating a growing demand for high-performance reconfigurable radio frequency (RF) devices. Low-phase-noise frequency references and narrow-band-pass filters are the key elements for emerging miniaturized multi-band RF transceivers [1]. In modern RF devices, high- Q filters and reference oscillators are realized using off-chip micro-electro-mechanical system (MEMS) resonators, such as quartz crystals along with thin-film bulk acoustic resonators and surface acoustic wave piezoelectric devices [2, 3]. These bulky components are limited in their frequency range, but satisfy strict phase noise specifications. The superior advantage of MEMS resonators is their high quality factors ($Q \sim 10^4 - 10^5$), which are orders of magnitude higher than those typical for conventional electronic components. A high Q contributes to improved frequency selectivity and phase stability along with a reduced level of insertion loss: $IL \sim \omega_0 / (Q \times \Delta\omega)$. For instance, a next-generation RF channel-select architecture requires $<0.1\%$ band-width filters, which can be realized using resonators with $Q > 10^4$.

Due to the material limitations of conventional silicon devices, wide band-gap semiconductor thin films, e.g. AlN [4, 5], SiC [6], ZnO [7] and diamond, were extensively explored for high ($Q \times f$) MEMS resonators. For this purpose, diamond shows great advantages over other materials, mainly due to its exceptional mechanical properties, e. g. an acoustic velocity of $v > 18000 \text{ m s}^{-1}$ ($v \sim 8000$ and $\sim 11500 \text{ m s}^{-1}$ reported for Si and SiC, respectively) along with a low predicted fundamental phonon scattering rate [8]. Given that the resonance frequency is proportional to the acoustic velocity, diamond thin films appear to be the best choice for high- Q RF micromechanical resonators.

2. Diamond based MEMS resonators

Single-crystalline diamond (SCD) beam resonators, having Q values exceeding 3×10^5 at 0.7 MHz, were recently demonstrated, showing promising results for emerging RF transducers [9]. However, SCD is too costly for most applications, and its use is rather limited by growth and processing issues. Fortunately, poly- (PCD) and nano- (NCD)

crystalline diamond thin films, with physical properties approaching those of SCD samples, are available via chemical vapor deposition (CVD) on low-cost silicon substrates [10]. Flexural beam resonators based on PCD thin films were reported by Sepulveda *et al* demonstrating $Q \sim 10^5$ at 0.3 MHz. These experiments were powered by detailed analyses of dissipation mechanisms in vibrating beams, in order to evaluate diamond as a potential material for high- Q RF MEMS applications [11].

The mechanical quality factor, Q , of a resonator is generally defined as:

$$Q^{-1} = \left(\omega_0 \frac{W}{W_D} \right)^{-1} = Q_c^{-1} + Q_g^{-1} + Q_{\text{intr}}^{-1}, \quad (1)$$

where W and W_D are the stored vibrational energy and the average dissipated power per cycle, respectively, and ω_0 is the resonant angular frequency. Among the major loss mechanisms, (i) the resonator clamping losses (Q_c^{-1}) and (ii) the viscous gas damping (Q_g^{-1}) are the most prevalent for the case of flexural beams. For such resonators in either an air or fluid environment, the viscous damping usually dominates [12]. However, for vacuum levels of < 1 mbar, the gas damping contribution is minimal and can be neglected [13].

Therefore, the clamping losses, defined as part of the vibration energy dissipated through elastic wave propagation into the substrate, can be identified as the dominant loss mechanism for the beams operating in a vacuum. A maximal achievable Q_c depends, in this case, on the oscillator geometry. For instance, $Q_c = 0.34 (L/h)^3$ is an approximation derived for a cantilever beam [14], where L and h are the length and the thickness of the beam, respectively. For more complicated resonator geometries, like disk-shaped oscillators, the analytical expression for Q_c is of greater complexity, comprising the Q dependencies on the support beam's material, thickness and radius, along with the order of vibrational mode [15]. The intrinsic loss mechanisms (Q_{intr}^{-1}), of which thermo-elastic dissipation [16], phonon-phonon interaction [17], internal friction and surface losses (e.g. due to surface/interface roughness) are prevalent, are mostly material dependent and relevant for practical consideration if the two above-mentioned dissipations (Q_c and Q_g) are strongly minimized.

Recently, advanced forms of resonating devices were utilized in order to realize high- $(Q \times f)$ mechanical oscillators via a substantial reduction of extrinsic and intrinsic losses [15]. In particular, the 'radial contour mode' diamond disk resonators with 'material-mismatched' Si stems were demonstrated with Q s exceeding 10^4 at 1.51 GHz [8]. Employing the volume-conserving whispering gallery modes (WGM), Q values as high as 10^5 at 0.5 GHz were reported on similar structures manifesting a further reduction in anchor/clamping losses [18].

While WGMs are characteristic for cylindrically symmetric systems, the sectoral spherical modes (SSM) are their equivalent in spherically symmetric systems (see figure 1(a)). Therefore, the logical step in the further development of electromechanical WGM-based transducers is the use of sphere-shaped resonators, which represent an ideal volume/energy conserving form. WGMs in microwave [19]

and optical [20] spherical oscillators have been extensively studied and well understood. However, there are only a few applied studies describing the electro-mechanical vibrations of solid spheres, mainly due to the difficulties in micro-fabrication and integration. Up to now, the major development of mechanical spherical resonators relates to gravitational wave antennas [21].

The vibrational modes of an uncoupled elastic sphere with uniform density ρ were considered in the classical work of Lamb [22]. Its eigenfunctions can be written in spherical coordinates (r, θ, φ) in terms of the Laplace spherical harmonics [23], $Y_{\ell m}$:

$$\Psi_{n\ell m}(r, \theta, \varphi) = (A_{n\ell}(r)\hat{r} + B_{n\ell}(r)R\nabla)Y_{\ell m}(\theta, \varphi), \quad (2)$$

where indexes ℓ and m define the number of nodal lines in the latitudinal ($\ell - |m|$) and longitudinal ($|m|$) directions, and eigenfunctions $A_{n\ell}(r)$ and $B_{n\ell}(r)$ determine the sphere motion in the radial and tangential directions, respectively, which depend on the radius R and the material parameters (ρ , shear modulus μ , and Poisson ratio ν).

These parameters fully describe the vibration problem. If the sphere is disturbed, e.g. by a broad-band electro-magnetic (EM) signal, it begins oscillating with eigenfrequencies $\omega_{n\ell m}$, and each spherical component of the EM field uniquely determines the effective force on the corresponding mode of the sphere. If the sphere is inhomogeneous, e.g. consists of a core and a shell made of different materials, and/or is supported by a stem, such a system cannot be treated analytically, and it is a subject of numerical simulations, e.g. by using a finite element method (FEM). The example of the FEM calculated, $S(\ell = 3, m = 3)$ vibrational mode carried out for the composite spherical oscillator is shown in figure 1(a). Such spheres, consisting of a silicon core ($\varnothing \sim 2.07$ mm) and an NCD external shell ($d \sim 100$ μm), have been studied in this work towards their resonant properties using laser Doppler vibrometry powered by FEM simulations and RF signal transient studies. The main aim of these investigations was to evaluate the potential of diamond based spherical resonators to be used as band-pass-filters and reference oscillators in modern communication devices.

3. Fabrication and experimental details

The NCD coated silicon spheres have been fabricated and chemo-mechanically polished using the technologies described in detail elsewhere [24]. Briefly, to obtain void-free, 100 μm thick NCD coatings, ultra-high-precision silicon spheres with a surface roughness < 3 nm (rms) were placed in an ultrasonically agitated nano-diamond-methanol suspension. With this seeding method, nano-particle nucleation densities as high as 10^{14} m^{-2} have been achieved. A uniform NCD coating was applied by continuously rotating the Si spheres during the CVD process carried out in a gas mixture of 1% methane in hydrogen at a deposition temperature of 700–860 $^\circ\text{C}$.

Following the polishing step, the spherical resonator was placed in the center of a cylindrical copper cavity (see figures 1(b), (c)), which was micro-machined in a specially

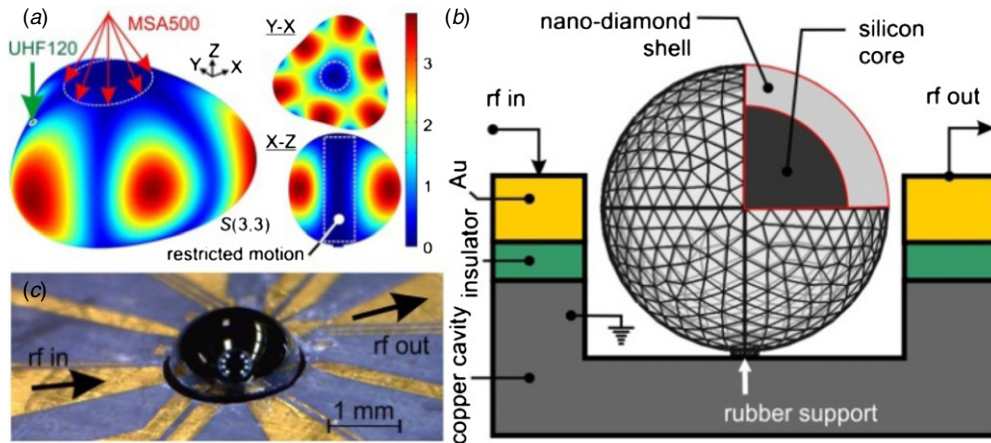


Figure 1. (a) The $S(3,3)$ sectoral vibration mode calculated for a resonator sphere mounted onto a fixed point support. The color-coding represents the magnitude of total displacement. On top of the 3D view image, the measurement arrangements for MSA500 and UHF120 laser vibrometers are shown. (b), (c) The NCD based spherical resonator: (b) the oscillator design and excitation/measurement schema; (c) an optical image of the resonator sphere ($\varnothing \sim 2.27$ mm) mounted in a 1.1 mm deep cylindrical copper cavity surrounded by Au/Cu radially-arranged electrodes emitting/receiving the RF-signal.

designed RF chip equipped with radially arranged Au/Cu electrodes.

A soft-rubber-like support (Poisson's ratio ~ 0.5) was used to fix the resonator in the center of the cavity in order (i) to minimize the support loss, and (ii) to realize conditions approaching the vibration of a support-free body. The gap of $150 \mu\text{m}$ separating the sphere equator and the electrodes was kept constant along the cavity circumference. The mechanical oscillations in the capacitively coupled resonator were excited using an electrical signal generated by either an external RF vector generator (R&S SMBV100A) or the internal generator of a network analyzer (R&S ZVL).

The mechanical resonant spectra were recorded using laser Doppler vibrometry. The scanning vibrometer (Polytec MSA500) was equipped with a 24 MHz displacement decoder with a resolution of $<0.1 \text{ pm Hz}^{-0.5}$, and a laser system having an optical output of $<1 \text{ mW}$ at $\lambda = 620 \text{ nm}$. A single-point, ultra-high frequency vibrometer (Polytec UHF120) was equipped with a 1.2 GHz displacement decoder with an amplitude resolution of $\sim 2 \text{ pm}$. Its laser system allows for an optical output of $\sim 5 \text{ mW}$ at $\lambda = 532 \text{ nm}$ and a spot size of $\varnothing < 1 \mu\text{m}$.

4. Results and discussion

4.1. Mechanical vibration spectra

The technical characteristics of scanning and single point vibrometers used in these studies allow us to carry out two complementary kinds of measurements. The MSA500 is capable of scanning a restricted area on top of the sphere (figure 1(a)), acquiring the majority of low-index vibration modes including the zonal [$S(\ell, m = 0)$, no longitudinal variations] and partly the tesseral harmonics [$S(\ell, m \neq \ell)$]. On the other hand, the sectoral harmonics [$S(\ell, m = \ell)$, no latitudinal variations] have a very restricted motion along the z-axis. In order to detect the sectoral harmonics precisely, a UHF120 system was employed. Due to the high optical power

Table 1. Parameters of the spherical resonator.

Parameter	Si	NCD
Sphere \varnothing , mm	2.070	2.270
Young's modulus, GPa	152	1050
Shear modulus, GPa	57	478
Material density, kg m^{-3}	2330	3550
Poisson's ratio	0.27	0.2
Conductivity, $\Omega \text{ cm}$	10–20	N.A.

and sub- μm spot size of the green laser, it allows for the detection of out-of-plane surface motion on the periphery of the sphere.

In figure 2, the experimental vibrational spectrum of a spherical resonator (in the bottom-half of the graph) is shown together with the FEM simulated spectrum (in the top-half of the graph). The vibrometry measurements and the simulations were performed on an ultra-precision NCD-shell/Si-core sphere. The resonator and materials parameters used for the evaluation are summarized in table 1. The experimental spectrum was measured by the scanning MSA500 vibrometer in the frequency range of 2–5 MHz with a resolution of $\sim 500 \text{ Hz}$. Amplitude averaging over 100 measurements was employed to collect all possible vibrational harmonics in one graph in order to compare the resonance positions with those appearing in the calculated spectra. As one can see in figure 2, the simulations fit the experimental data quite well, directly confirming the high precision of the resonator fabrication. In particular, characteristic doubled resonant peaks near the $S(3,0)$ zonal mode at $f_{3,0} \approx 3.18 \text{ MHz}$, together with the $f_{5,0} \approx 4.8 \text{ MHz}$ peak corresponding to the $S(5,0)$ mode, can be used for precise mode identification. The peak positions and the quality factors of selected zonal modes $S(\ell,0)$ determined experimentally are shown in table 2. $Q = f/\Delta f$ has been derived from a resonant peak fit using the Lorentz function, where Δf is the full width at half maximum of the resonance.

The results of a single-point vibrometry at the arbitrary lateral position relative to the z-axis of rotation are not

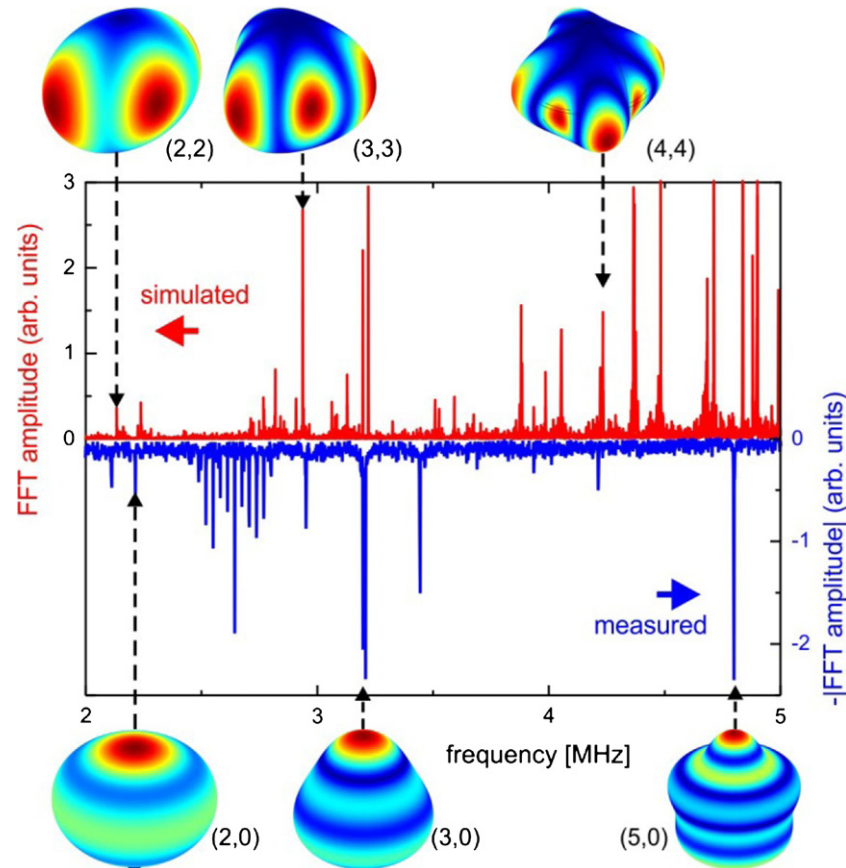


Figure 2. (a) The vibrational spectra of ultra-high-precision NCD-shell/Si-core spherical resonator with inner and outer diameters of 2.07 and 2.27 mm, respectively. The top half of the graph represents an FEM simulated spectrum; the bottom half of the graph shows the mirror image of the experimental one, recorded by a MSA500 vibrometer. Insets: the shapes of corresponding zonal [$S(\ell, 0)$] and sectoral [$S(\ell, m = \ell)$] modes used for the peak identification. The color-coding represents the magnitude of the total displacement field (in arbitrary units) of the oscillator body.

Table 2. Properties of the selected spheroidal modes.

Mode	Peak position, MHz Vibrom.	Q Vibrom.	Peak position, MHz Reflection	Peak position, MHz Transmission
$S(2, 2)$	2.11	4860*	2.08	2.15
$S(2, 0)$	2.22	2480	2.23	2.25
$S(3, 3)$	3.04	6902	3.07	3.04
$S(3, 0)$	3.20	3720	3.20	3.22
$S(4, 4)$	4.21	9355*	–	4.22
$S(5, 0)$	4.85	4798	–	4.86

* derived from the spectrum shown in figure 3.

straightforward for interpretation. As expected, the measured vibrational amplitudes depend strongly on the laser spot location and the local reflection conditions. The typical spectra obtained using the UHF120 vibrometer is shown in figure 3. Two sharp peaks, located at 2.11 and 4.21 MHz, correspond well to the sectoral $S(2,2)$ and $S(4,4)$ harmonics. The maximal $Q \sim 9300$ has been achieved *in air* for the $S(4,4)$ mode.

These SSM modes have a considerable *in plane* motion component, while the cylindrically-shaped central part remains relatively undistorted. The significant increase in Q -factor for a higher-order harmonic (see also table 2)

is, therefore, related to the specific distribution of the displacement in the sphere [see figure 1(a) for the $S(3,3)$]. Similar to disk resonators oscillating in the WGMs, SSMs are generated around the equator of the sphere, inducing minimal motion at the cylinder volume centered at the z -axis of rotation. For higher index modes, more energy is confined near the surface, within the NCD shell, thereby reducing the intrinsic losses in the Si-core, and especially in the Si/NCD interface area, where non-diamond inclusions adversely alter the acoustic velocity. The discussion on the structure of the diamond/silicon interface can be found elsewhere [10].

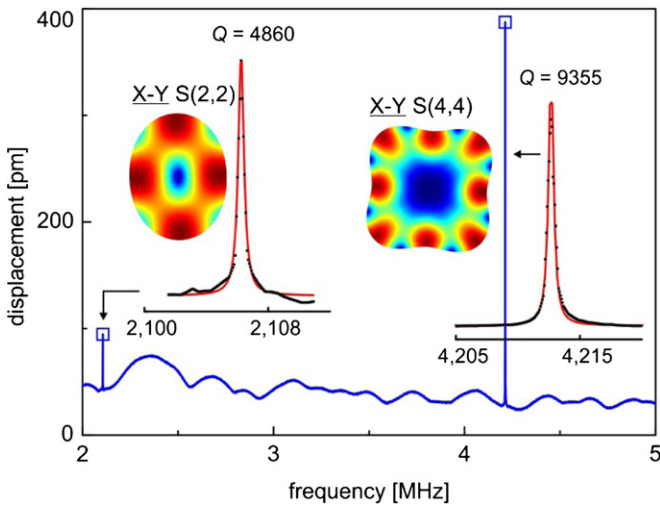


Figure 3. The out-of-plane vibrational spectrum of the spherical resonator recorded by the UHF120 vibrometer at the arbitrary lateral position. Insets: the fit of the resonant peaks shown together with the x - y plane cross-sections representing the (2, 2) and (4, 4) vibration modes. The resonant peaks were fitted using the Lorentz function in order to derive mechanical quality factors for the detected spheroidal $S(\ell, m)$ harmonics.

4.2. Electrical reflectance and transmission

The characterization of the spherical resonator was accomplished by reflection and transmission electrical measurements using a broad-band RF signal generated and detected by a network analyzer. Here, we assume that the input impedance of the spherical resonator has a pure capacitive character with the reactance of $X_c = (\omega C)^{-1}$. Due to the enormous gap size of $\sim 130 \mu\text{m}$, resulting in the measured capacitance of $C \sim 30\text{--}40 \text{ pF}$, the X_c value is high. Therefore, the resonator is not matched well to the 50Ω network, and the electrical measurement precision is quite restricted. However, certain conclusions can be drawn that are based on the direct comparison of the impedance and vibrometry spectra.

Examples of normalized reflection and transmission spectra are shown in figures 4(a) and (b), while figure 4(c) displays an electrical equivalent circuit and device geometry for the measured resonator system. One can see that characteristic peaks in the reflection spectrum correspond well to the main vibration modes shown in figure 2 and also in table 2. This indicates a higher EM energy loss at the positions corresponding to the resonant frequencies of the sphere. The transmitted signal is shown in figure 4(b). The resultant resonant peak positions are listed in table 2. Similar to the reflected signal, all the peaks corresponding to the low-index mechanical spheroidal eigenmodes can be recognized in the spectra in the range of 2–5 MHz. Therefore, both reflection and transmission measurements fit reasonably well to the resonant data obtained by the laser vibrometry.

On the other side, the quality factors derived from the transmission spectra are difficult to evaluate due to the weak signal conditions altering the results. Therefore, for the current configuration of the transducer, we assume that the mechanical Q values obtained by laser vibrometry do not differ

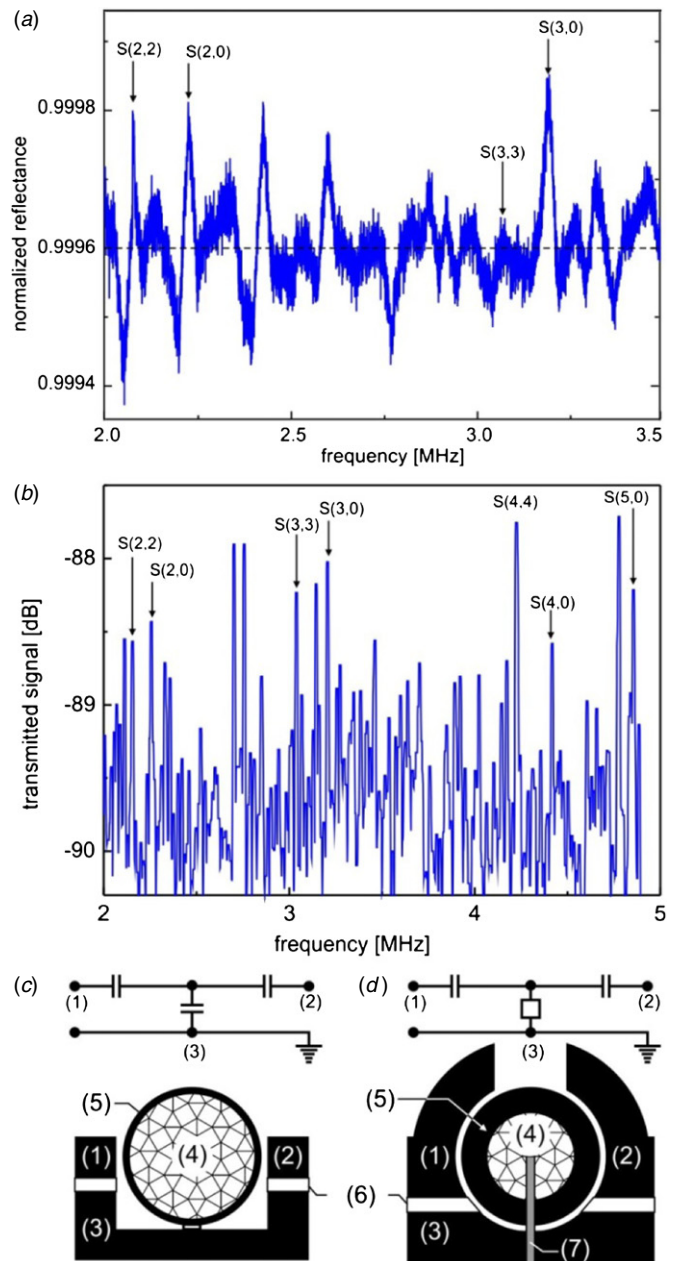


Figure 4. (a) Normalized reflectance and (b) transmission spectra of the spherical resonator system measured at a signal level of 20 dBm. Notes: only the selected zonal and sectoral modes are indicated in the spectra. (c), (d) The equivalent circuits and the device geometries shown for (c) the actual resonator and (d) prospective low-impedance system. [(1)—RF input; (2)—RF output; (3)—Cu cavity/ground; (4)—Si core; (5)—poly-C shell; (6)—insulator film; (7)—conducting stem].

significantly from the values measured electrically (see, for instance, [25]).

5. Final remarks and conclusions

In summary, the mechanical vibrations of the composite diamond-shell/Si-core spherical MEMS resonators were precisely measured and thoroughly analyzed. In order to obtain the vibration properties approaching the support-free elastic

sphere, the composite oscillators were mounted in the Cu-cavity using a soft-rubber-like support ($\nu \sim 0.5$). This method allowed for a convenient comparison of numerically simulated and experimentally recorded vibration spectra, along with a substantial decrease in support loss. It was demonstrated that due to the ultra-precision fabrication of the spheres, the calculated spectrum is in good agreement with the measured one, allowing for the exact identification of the vibrational modes.

It was also shown that the achievable quality factors strongly depend on the displacement distribution over the sphere volume, favoring the sectoral modes for use in high- Q devices. This is due to the specific nature of these modes, where mechanical SSMs are generated along the equator of the sphere shell (diamond), which induces minimal motion at the cylinder volume centered at the z -axis of rotation (consisting mostly of Si). Therefore, for the sectoral modes, the significant reduction of intrinsic/anchor losses in the Si-core and in the Si/NCD interface was achieved, resulting in mechanical $Q \sim 10^4$, measured for the sectoral $S(4,4)$ mode *in air*.

Much higher Q values might be achievable for SSMs in spherical resonators upon further improvements in the system design, which are presented in figure 4(d). Among them:

- growth of a thicker shell should lead to the confinement of the high-order SSMs within the homogeneous nano-diamond layer, thereby further reducing the intrinsic losses in the Si-core and in the high defect density interface area (see the discussion in 4.1);
- the high capacitive transducer impedance might be reduced by implementation of a conducting stem configuration, which would also allow for a precise self-centering of the sphere;
- even further reduction of the capacitive impedance can be achieved by the scaling of the sphere–electrode spacing down to 100–150 nm using a self-centering technique, followed by 5–6 times enlargement in the electrode square.

Acknowledgments

The authors would like to thank S Klingelmeier, D Brink and O Kappeler for the technical assistance and to acknowledge funding from the German Research Foundation (DFG) within the research grants RF-CUBE & Säulenresonator.

References

- [1] Nguyen C T 2005 Vibrating RF MEMS overview: applications to wireless communications *Proc. SPIE* **2005** 11–25
- [2] Tilmans H A C, De Raedt W and Beyne E 2003 MEMS for wireless communications: from RF-MEMS components to RF-MEMS-SiP *J. Micromech. Microeng.* **13** 139–63
- [3] van Beek J T M and Puers R 2012 A review of MEMS oscillators for frequency reference and timing applications *J. Micromech. Microeng.* **22** 013001
- [4] Sorokin B P, Kvashnin G M, Volkov A P, Bormashov V S, Aksenenkov V V, Kuznetsov M S, Gordeev G I and Telichko A V 2013 AlN/single crystalline diamond piezoelectric structure as a high overtone bulk acoustic resonator *Appl. Phys. Lett.* **102** 113507
- [5] Lebedev V, Heidrich N, Knöbber F, Sah R E, Pletschen W, Raynor B, Polyakov V, Cimalla V and Ambacher O 2012 Electrostatically coupled vibration modes in unimorph complementary microcantilevers *Appl. Phys. Lett.* **100** 124104
- [6] Perisanu S, Vincent P, Ayari A, Choueib M, Purcell S T, Bechelany M and Cornu D 2007 High Q factor for mechanical resonances of batch-fabricated SiC nanowires *Appl. Phys. Lett.* **90** 043113
- [7] Dong S R, Bian X L, Jin H, Hu N N, Zhou J, Wong H and Deen M J 2013 Electrically tunable film bulk acoustic resonator based on Au/ZnO/Al structure *Appl. Phys. Lett.* **103** 062904
- [8] Wang J, Butler J E, Feygelson T and Nguyen C T 2004 1.51 GHz nanocrystalline diamond micromechanical disk resonator with impedance-mismatched isolating support *Proc. 17th IEEE Int. Conf. on Micro Electro Mechanical Systems* pp 641–4
- [9] Ovarthaiyapong P, Pascal L M A, Myers B A, Lauria P and Bleszynski Jayich A C 2012 High quality factor single-crystal diamond mechanical resonators *Appl. Phys. Lett.* **101** 163505
- [10] Hees J, Heidrich N, Pletschen W, Sah R E, Wolfer M, Williams O A, Lebedev V, Nebel C E and Ambacher O 2013 Piezoelectric actuated micro-resonators based on the growth of diamond on aluminum nitride thin films *Nanotechnology* **24** 025601
- [11] Sepulveda N, Aslam D and Sullivan J P 2006 Polycrystalline diamond MEMS resonator technology for sensor applications *Diam. Relat. Mater.* **15** 398–403
- [12] Brueckner K, Niebelschuetz F, Tonisch K, Foerster C, Cimalla V, Stephan R, Pezoldt J, Stauden T, Ambacher O and Hein M A 2011 Micro- and nano-electromechanical resonators based on SiC and group III-nitrides for sensor applications *Phys. Status Solidi a* **208** 357–76
- [13] Knöbber F, Zürlig V, Heidrich N, Hees J, Sah R E, Baeumler M, Leopold S, Pätz D, Ambacher O and Lebedev V 2012 Static and dynamic characterization of AlN and nanocrystalline diamond membranes *Phys. Status Solidi a* **209** 1835
- [14] Yang J, Ono T and Esashi M 2002 *IEEE J. Microelectromech. Syst.* **11** 775
- [15] Hao Z and Ayazi F 2005 Support loss in micromechanical disk resonators *Proc. 18th IEEE Int. Conf. on Micro Electro Mechanical Systems* pp 137–41
- [16] Roszhart T V 1990 The effect of thermoelastic internal friction on the Q of micromachined silicon resonators *Solid-State Sens. Actuator Workshop Technical Digest* 13–16
- [17] Braginsky V B, Mitrofanov V P, Panov V I and Thorne K S 1985 *Systems with Small Dissipation* (Chicago: The University of Chicago Press)
- [18] Rocheleau T O, Naing T L, Zeying R and Nguyen C T 2012 Acoustic whispering gallery mode resonator with $Q > 109,000$ at 515 MHz *Proc. 25th IEEE Int. Conf. on Micro Electro Mechanical Systems* pp 672–5
- [19] Anstie J D, Hartnett J G, Tobar M E, Winterflood J, Cros D and Krupka J 2003 Characterization of a spherically symmetric fused-silica-loaded cavity microwave resonator *Meas. Sci. Technol.* **14** 286–93
- [20] Matsko A B and Ilchenko V S 2006 Optical resonators with whispering-gallery modes—part I: basics *IEEE J. Sel. Top. Quantum Electron.* **12** 3
- [21] Merkowitz S M and Johnson W W 1995 Spherical gravitational wave antennas and the truncated icosahedral arrangement *Phys. Rev. A* **51** 2546–58
- [22] Lamb H 1881 On the vibrations of an elastic sphere *Proc. Lond. Math. Soc.* **13** 189

- [23] MacRobert T M 1967 *Spherical Harmonics: An Elementary Treatise on Harmonic Functions with Applications* (Oxford: Pergamon Press)
- [24] Biener J *et al* 2009 Diamond spheres for inertial confinement fusion *Nucl. Fusion* **49** 112001
- [25] Manzanque T, Hernando-García J, Ababneh A, Schwarz P, Seidel H, Schmid U and Sánchez-Rojas J L 2011 Quality-factor amplification in piezoelectric MEMS resonators applying an all-electrical feedback loop *J. Micromech. Microeng.* **21** 025007